Bulletin of the Seismological Society of America, 89, 2, pp. 538–543, April 1999

Short Notes

Source–Receiver Reciprocity and Empirical Green's Functions from Chemical Blasts

by Robert L. Nowack and Wang-Ping Chen

Abstract We investigated source–receiver reciprocity in the context of empirical Green's functions (EGF) for chemical blasts. Theoretically, reciprocity holds between a purely explosive source and the divergence of the displacement field (dilation). Using a pair of large, delay-sequence mining blasts in southern Indiana, we carried out a pilot experiment in the field. Preliminary results show that reliable EGF can be obtained using reciprocity below a frequency threshold of about 2 Hz, where fine details in the source function are not critical. These results have applications for the characterization of seismic sources and wave propagation at local and regional distances using reciprocal geometries.

Introduction

The study of chemical explosions is important for the detection and discrimination of low-yield underground nuclear explosions. As background seismicity increases exponentially with decreasing event magnitude, large chemical explosions, ever present for mining, quarrying, and construction, become an important issue in seismic verification (e.g., Husebye and Dainty, 1996; Richards, 1997; Richards *et al.*, 1992; Sullivan, 1998).

Recently, there have been a number of studies on chemical explosions to characterize their sources and to investigate effects of seismic-wave propagation at regional distances. For instance, Smith (1989) deployed a temporary seismic array to study high-frequency signals from delay-sequence blasts at regional distances over a shield region. In conjunction with seismic recording of ground motion, Stump *et al.* (1996) made video images of mining blasts to constrain their source processes. Anandakrishnan *et al.* (1997) investigated seismic signals from cast blasting, a process in which an array of shots is detonated to cast rock into a pit.

Given the complexity of crustal and mantle structures, empirical Green's functions (EGF) are a practical approach to characterize seismic wave propagation at regional distances that, in turn, form a basis for obtaining reliable information of complex seismic sources along particular event-receiver paths. For instance, Smith (1993) used EGF in the context of isolating a single, large explosion hidden within a delay-sequence blast. EGF were obtained by recordings of simple explosions to characterize path effects due to seismic-wave propagation. Deconvolution was then applied to recordings of complex explosions to isolate source effects.

In practice, the utility of EGF is limited by the availability of suitable event-receiver geometries. It seems unlikely that EGF can be easily obtained by setting off chemical explosions at a suspected site of nuclear tests. On the other hand, if source–receiver reciprocity approximately holds for explosions, EGF can be obtained by setting off chemical explosions near permanent stations and receiving signals at temporary stations near the suspect site under inspection. This scenario is realizable because on-site inspection is an important provision of the Comprehensive Test Ban Treaty. To investigate the utility of seismic experiments involving reciprocity, we carried out a pilot experiment using mining blasts in southern Indiana, and the initial results are encouraging.

Review of Theoretical Developments

For a compact seismic source located at $\bar{x}^A$, the resulting displacement field at a receiver at $\bar{x}^B$ can be written as

$$u_i(\bar{x}^B, t) = M_{pq}(t) * \frac{\partial G_{ip}(\bar{x}^B, t \mid \bar{x}^A, t^A)}{\partial x_q^A},$$

where there are implied sums from 1 to 3 over the repeated indices p and q, $M_{pq}(t)$ is the moment tensor representation of the source-time function, G_{ip} is the Green's function, and * denotes convolution (e.g., Aki and Richards, 1980). For the Green's function, we follow the convention that the first index indicates the component of the displacement at the receiver with time variable t, and the second index indicates the component of the point force at the source with time

variable t^A. Notice that the spatial derivative of the Green's function is taken with respect to the source coordinates, representing oriented force couples.

For an explosive source, the moment tensor can be written as $M_{pq}(t) = M(t)\,\delta_{pq}$, where δ_{pq} is the Kronecker delta function. The displacement field is then

$$u_i\,(\bar{x}^B,\,t) \;=\; M^A\,(t) \;*\; \frac{\partial G_{ip}\,(\bar{x}^B,\,t \mid \bar{x}^A,\,0)}{\partial x_p^A}, \qquad (1)$$

where there is an implied sum from 1 to 3 on the index p. For simplicity, we have set the origin time of the source to be zero. This configuration is shown in Figure 1a. If the source is now placed at $\bar{x}^B$ and the receiver at $\bar{x}^A$ (Fig. 1b), then the resulting displacement field is

$$u_i\,(\bar{x}^A,\,t) \;=\; M^B\,(t) \;*\; \frac{\partial G_{ip}\,(\bar{x}^A,\,t \mid \bar{x}^B,\,0)}{\partial x_p^B}. \qquad (2a)$$

Under homogeneous boundary conditions (zero traction or zero displacement), reciprocity holds for the Green's function $G_{ip}\,(\bar{x}^A,\,t \mid \bar{x}^B,\,0) = G_{pi}\,(\bar{x}^B,\,t \mid \bar{x}^A,\,0)$, where the indices for spatial components and the source and receiver positions have been interchanged (e.g., Aki and Richards, 1980). Inserting this expression into (2a) gives

$$u_i\,(\bar{x}^A,\,t) \;=\; M^B\,(t) \;*\; \frac{\partial G_{pi}\,(\bar{x}^B,\,t \mid \bar{x}^A,\,0)}{\partial x_p^B}. \qquad (2b)$$

Although the source-receiver geometry is the same in (2b) as in (1), the spatial derivative of the Green's function is now taken with respect to the receiver location $\bar{x}^B$. Thus, the path effects due to wave propagation, written as spatial derivatives of the Green's function in equations (1) and (2b) are not equivalent.

The path effects are identical, however, for the divergence of the displacement field. The divergence of the field for (1) is

$$\frac{\partial u_i\,(\bar{x}^B,\,t)}{\partial x_i^B} \;=\; M^A\,(t) \;*\; \frac{\partial^2 G_{ip}\,(\bar{x}^B,\,t \mid \bar{x}^A,\,0)}{\partial x_i^B \partial x_p^A} \qquad (3a)$$

and that for (2b) is

$$\frac{\partial u_i\,(\bar{x}^A,\,t)}{\partial x_i^A} \;=\; M^B\,(t) \;*\; \frac{\partial^2 G_{pi}\,(\bar{x}^B,\,t \mid \bar{x}^A,\,0)}{\partial x_p^B \partial x_i^A}. \qquad (3b)$$

Because i and p are dummy indices that are summed over, the terms representing wave propagation in (3a) and (3b) are now equivalent. Thus, for an explosive point source, reciprocity holds for the divergence of the displacement field, which is the dilation (dilatation) or the fractional change in volume $\Delta V/V$.

A point explosion is simply a point source of pressure, related to the fractional volume change by the bulk modulus,

RECIPROCITY FOR EXPLOSIVE SOURCES

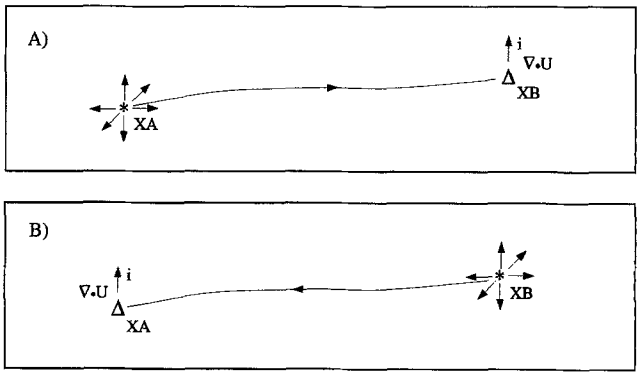

Figure 1. Reciprocity for explosive sources. (a) Explosive point-source at position XA with receiver at position XB. The ith displacement component is along the direction of the unit vector i. $\nabla \cdot U$ is the divergence (dilation or dilatation) of the displacement field. (b) Reciprocal geometry of (a). Reciprocity holds for the dilation field.

thus it is not surprising that reciprocity holds between a point explosion and the dilation field. For a fluid medium, this relationship is equivalent to the reciprocity for an explosive source and the pressure field recorded by a hydrophone. There is, however, an important difference between an elastic solid and fluid. At the free surface, the pressure (and hence dilation) is zero for a fluid, but it will generally not vanish for an elastic solid.

Ignoring tectonic release, explosions should theoretically generate only compressional waves at the source (e.g., Aki and Richards, 1980). Such a source can generate surface waves, particularly Rayleigh waves, and to a lesser extent other compressional-coupled shear waves due to *P-S* conversions at interfaces. However, for body waves in the far field, if such conversions are ignored, the wave field can be approximated as a plane wave of the scalar potential. Then the dilation and the displacement field are related to the scalar potential; and reciprocity should approximately hold for the displacement field generated by explosive sources, an observation tested in our pilot study to be discussed later.

The displacement generated from a delay-sequence explosive source can be written as

$$u_i\,(\bar{x},\,t) \;=\; \sum_{k=1}^{K} M_{pq}^k\,(t) \;*\; G_{ip,q}^k\,(\bar{x},\,t \mid \bar{x}_r,\,t_r),$$

where $M_{pq}^k(t)$ is the moment tensor of the kth shot in the blast and $G_{ip,q}^k$ is the spatial derivative of the Green's function for the kth shot. For the explosive component of the individual shots, the moment tensor is simply the product of the source-time function and the identity matrix. If the spatial separation between the shots are small, then the displacement field can be approximately written as

$$u_i\,(x,\,t) \;=\; B_{pq}\,(t) \;*\; G_{ip,q}\,(x,\,t \mid x_r^0,\,t_r^0),$$

where B_{pq} incorporates the time delay and the source-time function of individual shots in a delay-sequence blast, and the Green's function is evaluated for a centroidal reference location and time of the source.

Pilot Experiment

Field Configurations. Using blasts from large coal mining operations in the Sullivan–Greene counties of southern Indiana, we conducted a pilot seismic experiment in August of 1997 in which we deployed seismometers adjacent to two blast sites to set up a reciprocal source–receiver geometry (Fig. 2). The distance between the blast sites, the north pit and the southwest pit, is approximately 7.7 km. Each seismic station, marked as RS adjacent to the southwest pit and RN adjacent to the north pit in Figure 2, includes a three-component, 2-Hz seismometer (Mark Products L22D) and a Reftek data recorder with GPS clock.

Figure 3 shows details of the blast at the north pit. The shot array was located at the far western end of an east–west-trending high wall of about 33.5 m in height above the blasting pit. The seismometer was placed about 15.2 m back from the edge of the high wall to the northern side of the blast array. The site of the sensor was chosen to be nearby the blast and above the pit, but also well away from movement of heavy equipment. The blast was a 4 by 8 array of 32 individual shots, each at a depth of 12.8 m and with similar charge sizes. The separation between the individual shots was 6.7 m. Time delays with respect to the first shot (located on the southeast corner) were 25 msec in the north–south direction and 42 msec in the east–west direction (Fig. 3).

The configuration of the blast and location of our sensor at the southwest pit is similar (Fig. 4), except now that the array is located in the southwestern corner of the pit, just to the east of a north–south-trending high wall. The long axis of the shot array trends north–south, with the first shot being at the northeastern corner of the array (Fig. 4). At both pits, shots were detonated in the interseam shale formation between coal beds. The blast at the north pit has larger individual shot sizes than that at the southwestern pit, but precise yields are considered proprietary by the company that also requested to remain anonymous in activities unrelated to their commercial operations.

Data. Figure 5 shows a comparison of original, vertical-component seismograms of the two blasts recorded by nearby seismographs. The amplitudes have been unit normalized, and the initial times are with respect to the start of the recording data block for each trace. For both cases, the blast pattern itself is expected to generate a signal of approximately 0.5 sec in duration. However, the smaller individual shots (and thus smaller total yield) at the southwest pit resulted in a more compact-looking waveform recorded at nearby station RS (Fig. 5) than the slightly clipped signal observed at RN for the blast at the north pit.

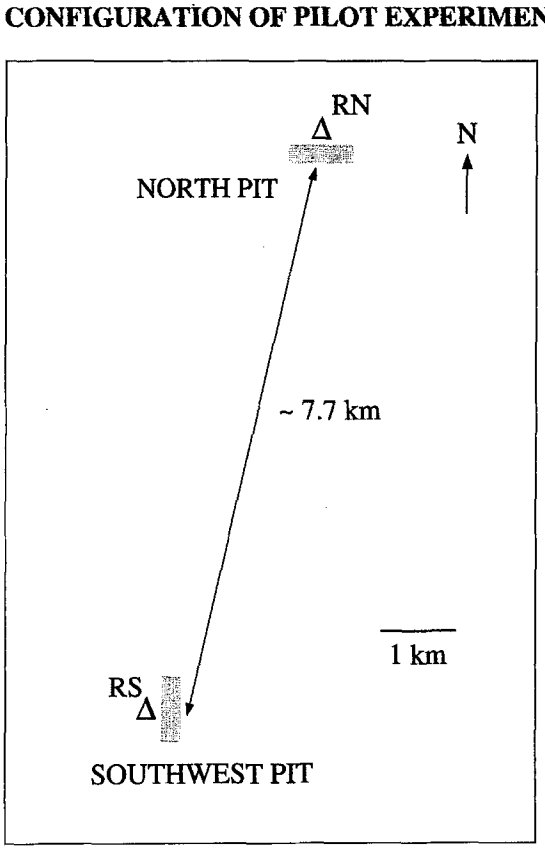

Figure 2. Configuration of pilot experiment with the delay-sequence sources located in the north pit and the southwest pit. The three-component seismographs are located at RS and RN.

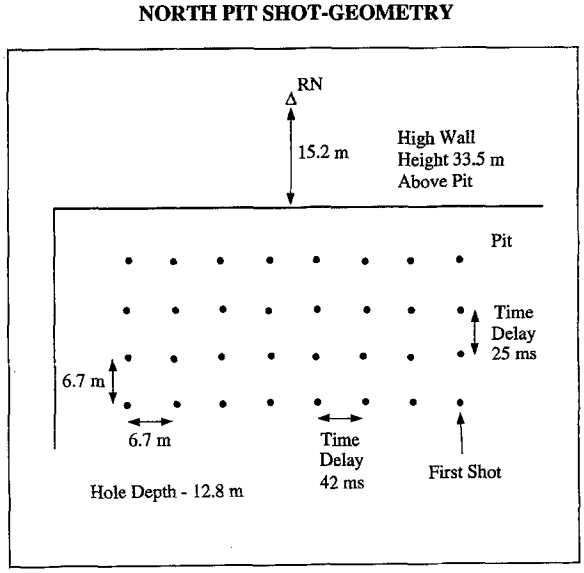

Figure 3. Experimental configuration of the north pit. The solid dots show the locations of the individual shots making up the delay-sequence blast. Station RN is located about 15.2 m from the high wall.

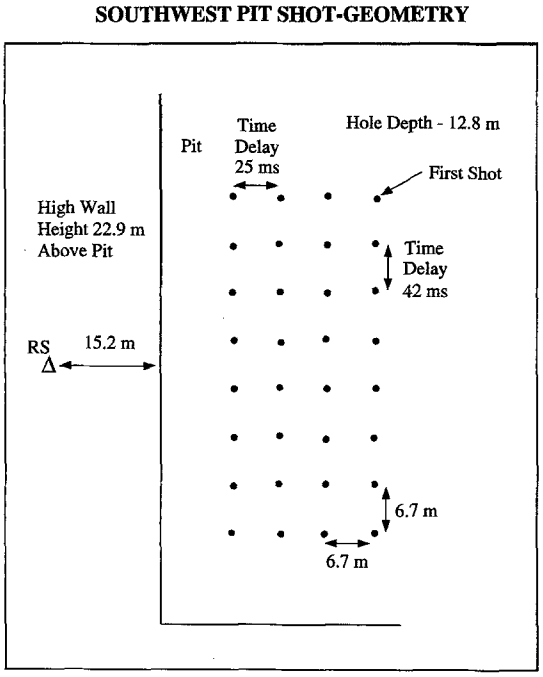

Figure 4. Experimental configuration of the southwest pit. The solid dots show the locations of the individual shots making up the delay-sequence blast. Station RS is located about 15.2 m from the high wall.

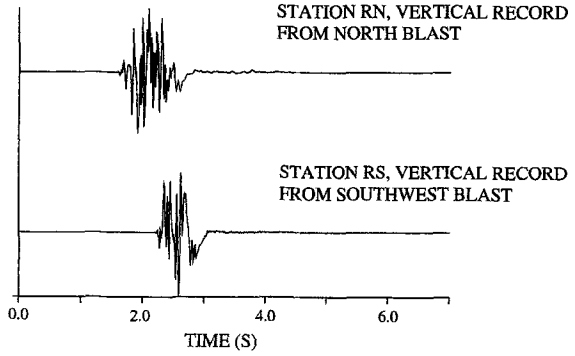

Figure 5. Ground velocity (vertical component) recorded by station RN due to the nearby blast at the north pit (*top*) and that recorded by station RS due to the nearby blast at the southwest pit (*bottom*). The amplitudes are unit normalized, and the zero times are with respect to the start of the recording data blocks.

At an epicentral distance of approximately 7.7 km, the general characteristics of vertical-component seismograms for the two blasts are similar (Fig. 6). The amplitudes are again unit normalized, and the initial times are with respect to the start of the recording data block for each trace. Large amplitudes occur near the onset of the wave trains that have a total duration of about 10 sec. In the later half of the signals, there is a dispersive wave train, probably Rayleigh

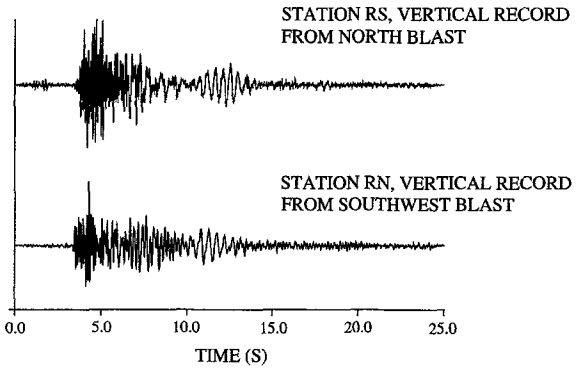

Figure 6. Ground velocity (vertical component) recorded by station RS due to the distant blast at the north pit (*top*) and that recorded by station RN due to the distant blast at the southwest pit (*bottom*). The amplitudes are unit normalized, and the zero times are with respect to the start of the recording data blocks.

waves, over the frequency range of 2 to 3 Hz. Because precise origin times (within about 5 to 10 msec) of each blast can be inferred from a nearby seismogram, travel times of the initial *P* wave give an apparent speed of about 4.5 km/sec.

Preliminary Analysis. For each of the three components, Figure 7 shows a comparison of seismograms recorded in a reciprocal geometry at five different frequency bands between 0.02 and 6 Hz. For each pair, the top trace is recorded at station RS for the blast at the north pit, while the lower trace is recorded at station RN for the blast at the southwest pit. For this geometry, the north and east components are within 15° of being radial and transverse. The bandpass filter used is a 6-pole, zero-phase Butterworth filter. Seismograms in each pair have been manually shifted so that peaks at the lowest frequency band are aligned. Also, for each frequency band, the trace amplitudes have been unit normalized.

There is generally good agreement in the waveforms for each pair up to a frequency of 2 Hz. This holds true for all three components of the ground motion (Fig. 7). Considering that the source wavelets have durations of about 1 sec (Fig. 5), it is not surprising that the agreement in each pair improves at lower frequencies (Fig. 7). At such frequencies, amplitudes of the Rayleigh waves are smaller (Figs. 6 and 7a), and the approximation of treating the blast pattern (~25 m × 45 m) and the source time function as a point source also improves. Notice that the ground motions at low frequencies (thus information about the seismic moment or yield of the source) are mainly contained in the leading half of the observed waveforms, for which reciprocity approximately holds (Fig. 7). Given the near-surface velocity of about 4.5 km/sec, the distant seismometer is within several wavelengths of the source for the lowest frequency components. Nonetheless, reciprocity apparently remains valid.

Observations shown in Figure 7 suggest that even without deconvolution to correct for effects of the source wave-

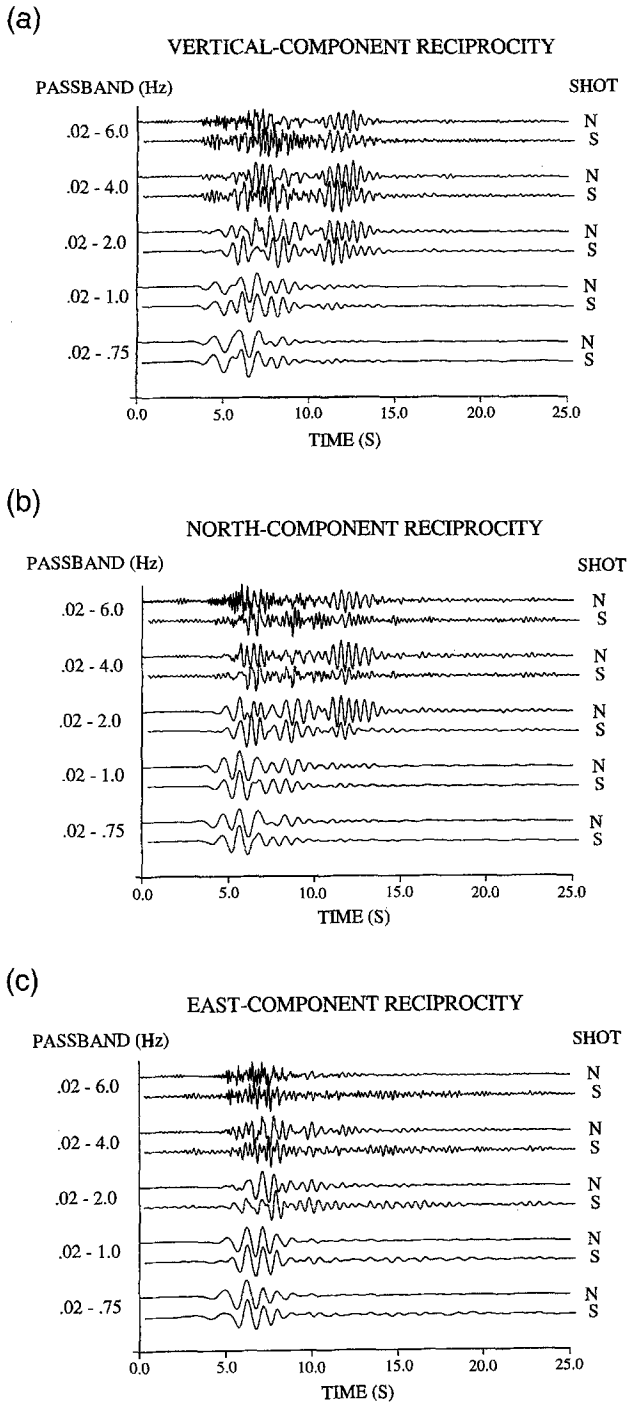

Figure 7. Comparisons of ground velocity at various frequencies for a reciprocal source–receiver geometry. The amplitudes are unit normalized for each frequency band, and the traces are aligned with respect to the lowest frequency band. Recordings are made at station RS due to the distant blast at the north pit (N) and station RN due to the distant blast at the southwest pit (S): (a) vertical components, (b) north components, and (c) east components.

lets, ground motions due to large mining blasts are approximately reciprocal at frequencies of up to 2 Hz. Because seismograms immediately adjacent to each blast are approximately the response of the high wall to the blast pattern in the near field, in principle, one should be able to estimate the shape of the source wavelet from these nearby seismograms. The results, in turn, could be used to remove the source effects in the EGF. Such a deconvolution process should improve the validity of using mining blasts for EGF at high frequencies. However, in this pilot study, such analysis cannot be performed because of a lack of an extensive set of on-scale, near-field data. As an alternative, the use of single-shot sources would also improve the reciprocity comparison at higher frequencies.

Conclusions

To test the potential of using reciprocity for obtaining empirical Green's functions at local to regional distances, we carried out an experiment using a pair of large delay-sequence mining blasts in southern Indiana at an epicentral distance of approximately 8 km. We found that below a threshold frequency of about 2 Hz, where the fine details in the source functions can be ignored, observed waveforms from reciprocal source–receiver geometries are very similar. This result is consistent with theoretical considerations in which reciprocity is expected between a purely explosive source and the dilation field. These results have applications to the characterization of seismic-wave propagation at local and regional distances by using reciprocal geometries from mining blasts.

Acknowledgments

We thank the mining company and engineers for their invaluable assistance in the field work. We also thank Scott Phillips for his careful review of the manuscript and Cliff Thurber for his assistance in acquiring the seismic equipment through IRIS PASSCAL. This study was completed with partial support from NSF Grants EAR96-14772 (RLN), EAR94-04809, EAR98-04718, and the Mid-America Earthquake Center (WPC).

References

Aki, K. and P. G. Richards (1980). *Quantitative Seismology: Theory and Methods,* Freeman, San Francisco, 932 pp.

Anandakrishnan, S., S. R. Taylor, and B. W. Stump (1997). Quantification and characterization of regional seismic signals from cast blasting in mines: a linear elastic model, *Geophys. J. Int.* **131,** 45–60.

Husebye, E. and A. Dainty (Editors) (1996). *Monitoring a Comprehensive Test Ban Treaty,* Kluwer Academic Publishers, Boston.

Richards, P. G. (1997). Seismological methods of verification and the International Monitoring System, in *The Comprehensive Test Ban Treaty: Issues and Answers, Occasional Paper 21, Cornell University Peace Studies Program,* M. McKinzie (Editor), Chap. 7, Cornell University Peace Studies Program, Cornell, New York.

Richards, P. G., D. A. Anderson, and D. W. Simpson (1992). A survey of blasting activity in the United States, *Bull. Seism. Soc. Am.* **82,** 1416–1433.

Smith, A. T. (1993). Discrimination of explosions from simultaneous mining blasts, *Bull. Seism. Soc. Am.* **83,** 160–179.

Smith, A. T. (1989). High-frequency seismic observations and models of chemical explosions: implications for the discrimination of ripple-fired mining blasts, *Bull. Seism. Soc. Am.* **79,** 1089–1110.

Stump, B. W., D. P. Anderson, and D. C. Pearson (1996). Physical constraints on mining explosions: synergy of seismic and video data with three dimensional models, *Seism. Res. Lett.* **67,** 9–24.

Sullivan, J. D. (1998). The Comprehensive Test Ban Treaty, *Phys. Today* **51,** 24–29.

Department of Earth and Atmospheric Sciences
Purdue University
West Lafayette, Indiana 47907
(R.L.N.)

Department of Geology
University of Illinois
Urbana, Illinois 61801
(W.-P.C.)

Manuscript received 1 September 1998.